ROBUST POSE ESTIMATION OF MOVING OBJECTS USING LASER CAMERA DATA FOR AUTONOMOUS RENDEZVOUS & DOCKING

[a]Farhad Aghili, [b]Marcin Kuryllo, [b]Galina Okouneva and [b]Don McTavish

[a]Canadian Space Agency, Space Technologies
6767 route de l'Aeroport, Saint-Hubert, QC, Canada J3Y 8Y9
Email:farhad.aghili@space.gc.ca
[b] Ryerson University, Department of Aerospace Engineering
350 Victor Street, Toronto
Ontario, Canada M5B 2K3
Email: (gokoune,mctavish)@ryerson.ca

KEY WORDS: laser camera system, pose estimation, pose tracking, iterative closest point algorithm, extend Kalman filter, point cloud

ABSTRACT:

Different perception systems are available for the estimation of the pose (position and orientation) of moving objects. For space applications, an active vision system such as Laser Camera System (LCS) developed by Neptec Design Group (Ottawa, Canada) is preferable for its proven robustness in harsh lighting conditions of space. Based on LCS data, this paper presents results of integration of a Kalman filter (KF) and an Iterative Closest Point (ICP) algorithm in a closed-loop configuration. The initial guess for the ICP is provided by state estimate propagation of the Kalman filer. This way, the pose estimation of moving objects becomes more accurate and reliable in case when LCS does not deliver reliable data for a number of frames and the last known pose, used as an initial guess for the next one, is outside the ICP convergence range. In this case, the proposed algorithm automatically relies more on the dynamics model to estimate the pose, and vice versa. The Kalman filter, as a part of the integrated framework, is capable of not only estimating the target's states, but also its inertial parameters. The convergence properties of this framework are demonstrated by experimental results from real-time scanning of a satellite model attached to a manipulator arm, which is driven by a simulator according to orbital and attitude dynamics. These results proved robust pose tracking of the satellite only if the Kalman filter and ICP are in the closed-loop configuration.

1 INTRODUCTION

The paradigm of on-orbit, robotic servicing of stranded spacecraft has attracted many researchers [Zimpfer and Spehar, 1996, Yoshida, 2003, **?**]. To verify and to demonstrate the research results and the developments, several missions have already been performed and more will be in the future. An overview of the past, current, and future missions is presented in [Rekleitis et al., 2007]. For the successful accomplishment of such a mission, it is essential for the servicer spacecraft to have an accurate, real-time estimate of the motion of the *free-falling* target spacecraft and to be able to reliably predict the location of the target in near future.

There are different vision systems capable of estimating the pose (position and orientation) of moving objects. However, among them, an active vision system such as the Neptec Laser Camera System (LCS) is preferable because of its robustness in face of the harsh lighting conditions of space [Samson et al., 2004]. As verified during the STS-105 space mission, the 3D imaging technology used in the LCS can indeed operate in space environment. The use of laser range data has also been proposed for the motion estimation of *free-floating* space objects [Lichter and Dubowsky, 2004]. All vision systems, however, provide discrete and noisy pose data at relatively low rate, which is typically 1 Hz.

Taking advantage of the simple dynamics of a free-floating object, which is not acted upon by any external force or moment, researchers have employed different observers to track and predict the motion of a target satellite [Masutani et al., 1994, Aghili

and Parsa, 2009]. In some circumstances, e.g., when there are occlusions, no observation data are available. Therefore, long-term prediction of the motion of the object is needed for planning such operations as autonomous grasping of targets.

This work is focused on the integration of an Kalman filter and an ICP algorithm in a closed-loop configuration for accurate and reliable pose estimation of a moving object. In the conventional pose estimation algorithm, the range data from the LCS along with the surface model of the target satellite, or CAD-generated surface model, are used by the ICP algorithm to estimate the target pose. The estimation can be made more robust by placing the ICP and the KF estimator in a closed-loop configuration, wherein the initial guess for the ICP is provided by the estimate prediction. The KF estimator is designed so that it can estimate not only the target's states, but also its dynamic parameters. Specifically, the dynamics parameters are the ratios of the moments of inertia of the target, the location of its center of mass, and the orientation of its principal axes. Not only does this allow long-term prediction of the motion of the target, which is needed for motion planning, but also it provides accurate pose feedback for the control system when there are blackout, i.e., no observation data are available. We use the Euler-Hill equations [Kaplan, 1976] to derive a discrete-time model that captures the evolution of the relative translational motion of a tumbling target satellite with respect to a chaser satellite which is freely falling in a nearby orbit.

2   THE ICP ALGORITHM

This section reviews the basic Iterative Closest Point (ICP) algorithm which is an iterative procedure minimizing a distance between points in one set and the closest points, respectively, in the other. Suppose that we are given with a set of 3-D points data $\mathcal{D}$ that corresponds to a single shape represented by *model set* $\mathcal{M}$. It is known that for each point $d_i \in \mathbb{R}^3$ from the 3-D points data set $\mathcal{D}$, there exists at least on point on the surface of $\mathcal{M}$ which is closer to d_i than other points in $\mathcal{M}$ [Simon et al., 1994]. Assuming that the rigid transformation (R', r') is roughly known, where r' and R' are the translation vector and rotation matrix, respectively. Then, the problem of finding the correspondence between the two sets can be formally expressed by

$$c_i = \arg \min_{c_k \in \mathcal{M}} \|(R'd_i + r') - c_k\| \qquad \forall i = 1, \cdots, m, \quad (1)$$

and then set $\mathcal{C} = \{c_1 \cdots c_m\}$ is formed accordingly. Now, we have two independent sets of 3-D points $\mathcal{C}$ and $\mathcal{D}$ both of which corresponds to a single shape. The problem is to find a fine alignment (R,t) which minimizes the distance between these two sets of points [Besl and McKay, 1992]. This can be formally stated as

$$\epsilon = \frac{1}{m} \min_{r, R} \sum_{i=1}^{m} \|Rd_i + r - c_i\|^2 \qquad \forall c_i \in \mathcal{C}, d_i \in \mathcal{D}. \quad (2)$$

which has a closed-form solution [Faugeras and Herbert, 1986]. The ICP-based matching algorithm may proceed through the following steps:

1. Given a coarse alignment (R', r'), find closest point pairs $\mathcal{C}$ from scan 3-D points set $\mathcal{D}$ and model set $\mathcal{M}$ according to (1).

2. Calculate the fine alignment translation (R, r) minimizing the mean square error the distance between two data sets $\mathcal{D}$ and $\mathcal{C}$ according to (2)

3. Apply the incremental transformation from step 2 to step 1.

4. Iterate until the error norm $\|\epsilon\|$ is less than a threshold.

It has been shown that the above ICP algorithm is guaranteed to converge to a local minimum [Besl and McKay, 1992]. However, a convergence to a global minimum depends on a good initial alignment [Amor et al., 2006]. In pose estimation of moving objects, "good" initial poses should be provided at the beginning of every ICP iteration. The initial guess for the pose can be taken from the previous estimated pose obtained from the ICP [Samson et al., 2004]. However, this can make the estimation process fragile when dealing with relatively fast moving target. This is because, if the ICP does not converge for a particular pose, e.g., due to occlusion, in the next estimation step, the initial guess of the pose may be too far form its actual value. If the initial pose happens to be outside the global convergence region of the ICP process, from that point on, the pose tracking is most likely lost for good. The estimation can be made more robust by placing the ICP and a dynamic estimator in a closed-loop configuration, whereby the initial guess for the ICP is provided by the estimate prediction of the moving object. The following sections described design of a Kalman filter which will be capable of not only estimating the states but also and parameters of a free-floating object.
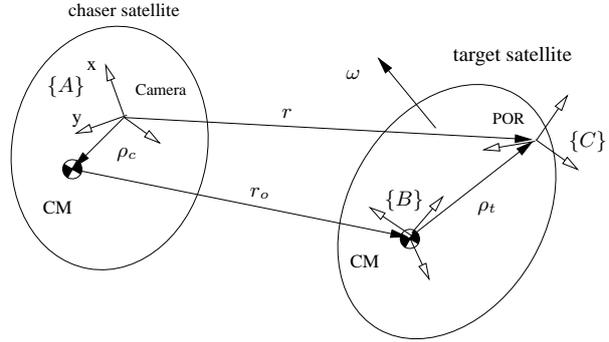

Figure 1: The body-diagram of chaser and target satellites moving in neighboring orbits

3   DYNAMIC ESTIMATOR

3.1   Modelling

Fig. 1 illustrates the chaser and the target satellites as rigid bodies moving in orbits nearby each other. Coordinate frames $\{A\}$ and $\{B\}$ are attached to the chaser and the target, respectively. The origin of $\{B\}$ is located at the target centre of mass (CM) while that of $\{A\}$ has an offset ρ_c with respect to the CM of the chaser. The axes of $\{B\}$ are oriented so as to be parallel to the principal axes of the target satellite. Coordinate frame $\{C\}$ is fixed to the target at its point of reference (POR) located at ρ_t from the origin of $\{B\}$; it is the pose of $\{C\}$ which is measured by the laser camera. We further assume that the target satellite tumbles with angular velocity ω. Also, notice that coordinate frame $\{A\}$ is not inertial; rather, it moves with the chaser satellite. In the following, quantities ρ_t and ω are expressed in $\{B\}$, while ρ_c is expressed in $\{A\}$.

The orientation of $\{B\}$ with respect to $\{A\}$ is represented by the unit quaternion q. Below, we review some basic definitions and properties of quaternions used in the rest of the paper. Consider quaternion q_1, q_2, q_3, and their corresponding rotation matrix R_1, R_2, and R_3. The operators $\otimes$ and $\odot$ are defined as

$$[a\otimes] \triangleq \begin{bmatrix} -[a_v \times] + a_o I_3 & a_v \\ -a_v^T & a_o \end{bmatrix}, [a\odot] \triangleq \begin{bmatrix} [a_v \times] + a_o I_3 & a_v \\ -a_v^T & a_o \end{bmatrix}.$$

Where a_o and a_v are the scalar and vector parts of quaternion a, respectively, and $[a_v \times]$ is the cross-product matrix of a_v. Then, $q_3 = q_2 \otimes q_1 = q_1 \odot q_2$, corresponds to product $R_3 = R_1 R_2$. Consider a small quaternion perturbation

$$\delta q = q \otimes \bar{q}^* \qquad (3)$$

where q represents the rotation of the target satellite with respect to the chaser satellite. Then, adopting a linearization technique similar to [Lefferts et al., 1982], one can linearize the above equation about the estimated states $\bar{q}$ and $\bar{\omega}$ to obtain

$$\frac{d}{dt}\delta q_v \approx -\bar{\omega} \times \delta q_v + \frac{1}{2}\delta\omega \qquad (4)$$

Dynamics of the rotational motion of the target satellite can be

expressed by Euler's equation as

$$\dot{\omega} = \psi(\omega) + J\varepsilon_\tau, \quad \text{where} \quad \psi(\omega) = \begin{bmatrix} p_x \omega_y \omega_z \\ p_y \omega_x \omega_z \\ p_z \omega_x \omega_y \end{bmatrix}, \quad (5)$$

where $J = \text{diag}\left(1, I_{xx}/I_{yy}, I_{xx}/I_{zz}\right)$; $p_x = (I_{yy} - I_{zz})/I_{xx}$, $p_y = (I_{zz} - I_{xx})/I_{yy}$, and $p_z = (I_{xx} - I_{yy})/I_{zz}$; I_{xx}, I_{yy}, and I_{zz} are the principal moments of inertia of the target satellite; ε_τ is a torque disturbance for unit inertia, and $p^T = \begin{bmatrix} p_x & p_y & p_z \end{bmatrix}$. Linearizing (5) about $\bar{\omega}_k$ and $\bar{p}$ yields

$$\frac{d}{dt}\delta\omega = A(\bar{\omega}_k, \bar{p})\delta\omega + B(\bar{\omega}_k)\delta p + J\varepsilon_\tau, \quad (6)$$

$$A(\omega) = \frac{\partial\psi}{\partial\omega} = \begin{bmatrix} 0 & p_x \omega_{z_k} & p_x \omega_{y_k} \\ p_y \omega_{z_k} & 0 & p_y \omega_{x_k} \\ p_z \omega_{y_k} & p_z \omega_{x_k} & 0 \end{bmatrix}$$

$$B(\omega) = \frac{\partial\psi}{\partial p} = \text{diag}\begin{bmatrix} \omega_y \omega_z & \omega_x \omega_z & \omega_x \omega_y \end{bmatrix}.$$

Let $x = \text{col}(q_v, \omega, p)$ describe the part of the system states pertaining to the rotational motion. Then, from (4) and (6), we have

$$\frac{d}{dt}\delta x = \begin{bmatrix} -[\bar{\omega}_k \times] & \frac{1}{2}I_3 & 0_{3\times3} \\ 0_{3\times3} & A(\bar{\omega}_k, \bar{p}_k) & B(\bar{\omega}_k) \\ 0_{3\times3} & 0_{3\times3} & 0_{3\times3} \end{bmatrix}\delta x + \begin{bmatrix} 0_{3\times1} \\ J\epsilon_\tau \\ 0_{3\times1} \end{bmatrix}. \quad (7)$$

In addition to the inertia of the target satellite, the location of its CM and the orientation of the principal axes η_v are uncertain. Note that quaternion η represents the orientation of frame $\{C\}$ w.r.t. frame $\{B\}$. Now, let vector $\theta = \text{col}(\rho_t, ; \eta_v)$ contains the additional unknown parameters. Then

$$\dot{\theta} = 0 \quad (8)$$

The evolution of the relative distance of the two satellites can be described by *orbital mechanics*. Let the chaser move on a circular orbit at an angular rate of n defined as $n^T = \begin{bmatrix} 0 & 0 & n_z \end{bmatrix}$. Further, assume that vector r_o denotes the distance between the CMs of the two satellites expressed in $\{A\}$, and that $v_o = \dot{r}_o$. Then, if $\{A\}$ is orientated so that its x-axis is radial and pointing outward, and its y-axis lies on the orbital plane, the translational motion of the target can be expressed as [Breakwell and Roberson, 1970, Kaplan, 1976]

$$\dot{v}_o = -2n \times v_o + \phi(r_o, n) + \epsilon_f. \quad (9)$$

Here, ϵ_f is the force disturbance for a unit mass, and acceleration term ϕ is due to the effect of orbital mechanics and can be linearized as $\phi^T(r_o, n) \approx [3n_z^2 r_{o_x} \quad 0 \quad -n_z^2 r_{o_z}]$. Denoting the states of the translational motion with $y = \text{col}(r_o, v_o)$, one can derive the corresponding dynamics model as

$$\frac{d}{dt}\delta y = \begin{bmatrix} 0_{3\times3} & I_3 \\ N & -2[n\times] \end{bmatrix}\delta y + \begin{bmatrix} 0_{3\times1} \\ \epsilon_f \end{bmatrix} \quad (10)$$

where

$$N \triangleq \frac{\partial\phi}{\partial r_o} = \begin{bmatrix} 3n_z^2 & 0 & 0 \\ 0 & 0 & 0 \\ 0 & 0 & -n_z^2 \end{bmatrix}.$$

3.2 Discrete Model

In order to take into account the composition rule of quaternion, the states to be estimated by the Kalman filter have to be redefined as $x_k = \text{col}(\delta q_{v_k}^T, \omega_k, p_k)$, $y_k = \text{col}(r_{o_k}, v_{o_k})$, and $\theta_k = \text{col}(\rho_{t_k}, \delta\eta_{v_k})$, where

$$\delta\eta = \bar{\eta}^* \otimes \eta.$$

Assuming $\chi \triangleq \text{col}(x, y, \theta)$, one can combine the nonlinear equations (5), (8) and (9) in the standard form as $\dot{\chi} = f(\chi, \epsilon)$, where $\epsilon = \text{col}(\epsilon_\tau, \epsilon_f)$. Moreover, setting the linearized systems (7), (8) and (10) in the standard state-space form $\dot{\chi} = \mathcal{A}\chi + \mathcal{B}\epsilon$, the equivalent discrete-time system can be written as

$$\chi_{k+1} = \Phi_k \chi_k + \epsilon_k. \quad (11)$$

Here the solution to the state transition matrix Φ_k and discrete-time process noise $Q_k = E[\epsilon_k \epsilon_k^T]$ can be obtained based on the van Loan method as $\Phi_k = D_{22}^T$ and $Q_k = \Phi_k D_{12}$, where

$$D = \begin{bmatrix} D_{11} & D_{12} \\ 0 & D_{22} \end{bmatrix} = \exp\left(\begin{bmatrix} -\mathcal{A} & \mathcal{B}\Sigma_\epsilon\mathcal{B}^T \\ 0 & \mathcal{A}^T \end{bmatrix} T\right)$$

with T being the sampling time and $\Sigma_\epsilon = E[\epsilon\epsilon^T] = \text{diag}(\sigma_\tau^2 I_3, \sigma_f^2 I_3)$. It should be noted that the $\mathcal{B}$ matrix depends on the inverse of the inertia matrix J, which can be generated from the estimated parameters by

$$\hat{J}_k = \text{diag}\left(1, \frac{1-\bar{p}_{y_k}}{1+\bar{p}_{x_k}}, \frac{1+\bar{p}_{z_k}}{1-\bar{p}_{x_k}}\right).$$

4 OBSERVATION

4.1 Sensitivity Matrix and Propagation of Measurement Noise

Let quaternion μ represent the orientation of frame $\{C\}$ w.r.t. frame $\{A\}$. Then, output of the vision system is

$$\text{pose meas.} \equiv \begin{bmatrix} r \\ \mu \end{bmatrix}, \quad \text{where} \quad \mu = \eta \otimes q.$$

Therefore, the observation vector is defined as

$$z = h(x) + \begin{bmatrix} v \end{bmatrix}, \quad (12)$$

where $z = \text{col}(z_1, z_2)$, $h = \text{col}(h_1, h_2)$, $v = \text{col}(v_1, v_2)$, and v_1 and v_2 are additive measurement noise processes, and

$$h_1 \triangleq r - \bar{r} = \delta r_o + R(q)\rho_t - R(\bar{q})\bar{\rho}_t \quad (13)$$

$$h_2 \triangleq \left(\bar{\eta}^* \otimes \mu \otimes \bar{q}^*\right)_v = \left(\delta\eta \otimes \delta q\right)_v = \left(\delta q \odot \delta\eta\right)_v. \quad (14)$$

The Extended Kalman filter (EKF) also requires the linearization of the above observation equations. The following partial derivatives are obtained from (13) and (14)

$$\frac{\partial h_1}{\partial\delta q_v} = -R(\bar{q})[\rho_t\times], \qquad \frac{\partial h_1}{\partial\delta\rho_t} = R(\bar{q}),$$

$$\frac{\partial h_2}{\partial\delta q_v} = -[\delta\eta_v\times] + \delta\eta_o I_3 - \delta q_o^{-1}\delta\eta_v \delta q_v^T,$$

$$\frac{\partial h_2}{\partial\delta\eta_v} = [\delta q_v\times] + \delta q_o I_3 - \delta\eta_o^{-1}\delta q_v\delta\eta_v^T.$$

In view of the above partials and neglecting the small terms, i.e., $\delta\eta_v\delta q_v^T \approx 0$, we can write the expression of the sensitivity matrix as

$$H_k = \begin{bmatrix} -2R(\bar{q})[\rho_{t_k}\times] & 0_{3\times 6} & I_3 & 0_{3\times 3} \\ -[\delta\eta_{v_k}\times] + \delta\eta_{o_k}I_3 & & 0_{3\times 12} & \\ R(\bar{q}) & 0_{3\times 3} & & \\ 0_{3\times 3} & [\delta q_{v_k}\times] + \delta q_{o_k}I_3 & & \end{bmatrix}.$$

Here we assume that $\delta\eta_v$ is sufficiently small so that $\delta\eta_o$ can be unequivocally obtained from $\delta\eta_o = (1 - \|\delta\eta_v\|^2)^{1/2}$.

Moreover, as shown in [Aghili and Parsa, 2009], in the case of isotropic orientation noise, i.e., $\Sigma_{q_v} = \sigma_{q_o}^2 I_3$, the equation of the covariance is drastically reduced to $E[v_2 v_2^T] = \sigma_{q_o}^2 I_3$.

4.2 Filter design

Recall that δq_v is a small deviation from the the nominal trajectory $\bar{q}$. Since the nominal angular velocity $\bar{\omega}_k$ is assumed constant during each interval, the trajectory of the nominal quaternion can be obtained from

$$\bar{q}(t) = e^{\frac{1}{2}(t-t_0)\bar{\omega}_k\otimes}\bar{q}(t_0) \implies \bar{q}_k = e^{\frac{1}{2}T\hat{\omega}_{k-1}\otimes}\hat{q}_{k-1}.$$

However, since η is a contact variable, we can say $\bar{\eta}_k = \hat{\eta}_{k-1}$. The EKF-based observer for the associated noisy discrete system (11) is given in two steps: (i) estimate correction

$$K_k = P_k^- H_k^T \left(H_k P_k^- H_k^T + S_k \right)^{-1} \tag{15a}$$

$$\hat{\chi}_k = \hat{\chi}_k^- + K\left(z_k - h(\hat{\chi}_k^-)\right) \tag{15b}$$

$$P_k = \left(I - K_k H_k \right) P_k^- \tag{15c}$$

and (ii) estimate propagation

$$\hat{\chi}_{k+1}^- = \hat{\chi}_k + \int_{t_k}^{t_{k+1}} f(\chi(t),0)\,dt \tag{16a}$$

$$P_{k+1}^- = \Phi_k P_k \Phi_k^T + Q_k \tag{16b}$$

and the quaternions are computed right after the innovation step (15b) from

$$\hat{q}_k = \delta\hat{q}_k \otimes \bar{q}_k = \begin{bmatrix} \delta\hat{q}_{v_k} \\ \left(1 - \|\delta\hat{q}_{v_k}\|^2\right)^{1/2} \end{bmatrix} \otimes e^{\frac{1}{2}T[\hat{\omega}_{k-1}\otimes]}\hat{q}_{k-1},$$

where $\underline{\omega}^T = [\omega^T \;\; 0]$, and

$$\hat{\eta}_k = \delta\hat{\eta}_k \odot \bar{\eta}_k = \begin{bmatrix} \delta\eta_{v_k} \\ \left(1 - \|\eta_{v_k}\|^2\right)^{1/2} \end{bmatrix} \odot \hat{\eta}_{k-1}.$$

4.3 ICP Initial Guess

Having obtained the estimate of the full states and parameters at a given point in time, one can integrate the dynamics model to predict the ensuing motion of the target satellite from that point on. The point-cloud data produced by the LCS is processed by an *Iterative Closet Point* (ICP) algorithm to estimate the pose of the target. The ICP basically is a search algorithm which tries to find the best possible match between the 3-D data of the LCS and a model within the neighborhood of the previous pose. In other words, the LCS sequentially estimates the current pose based on

(a) ICP takes initial guess from the last pose estimate
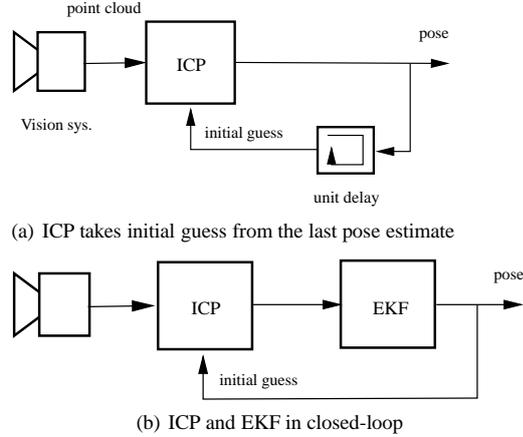

(b) ICP and EKF in closed-loop

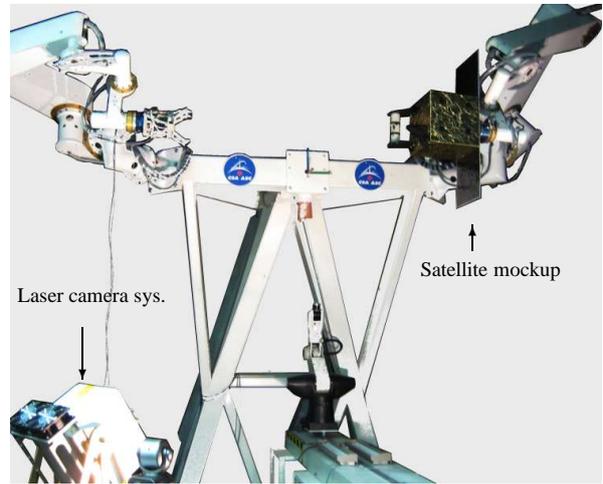Figure 2: Different configurations for tracking a moving object.

Figure 3: The experimental setup.

the previous one. That makes the estimation process fragile. This is because if the ICP does not converge for a particular pose, then, in the next estimation step, the initial guess of the pose may be far form the actual one. If the initial pose occurs to be outside the convergence region of the ICP process, from that point on the pose tracking is lost for good.

Fig. 2 illustrates the ICP and the adaptive predictor in a closed-loop configuration, where the initial guess for the ICP is provided by the predictor. The advantage of this configuration is twofold:

1. The convergence rate of the ICP is improved as the predictor provides a more accurate pose compared to just taking the previous pose estimate.

2. The pose tracking process becomes inherently robust, because if the ICP does not converge the predictor can still provide a good initial guess for the forthcoming ICP steps.

5 EXPERIMENT

In this section, experimental results are presented that show comparatively the performance of the pose estimation with and with-

(a) The satellite CAD model.

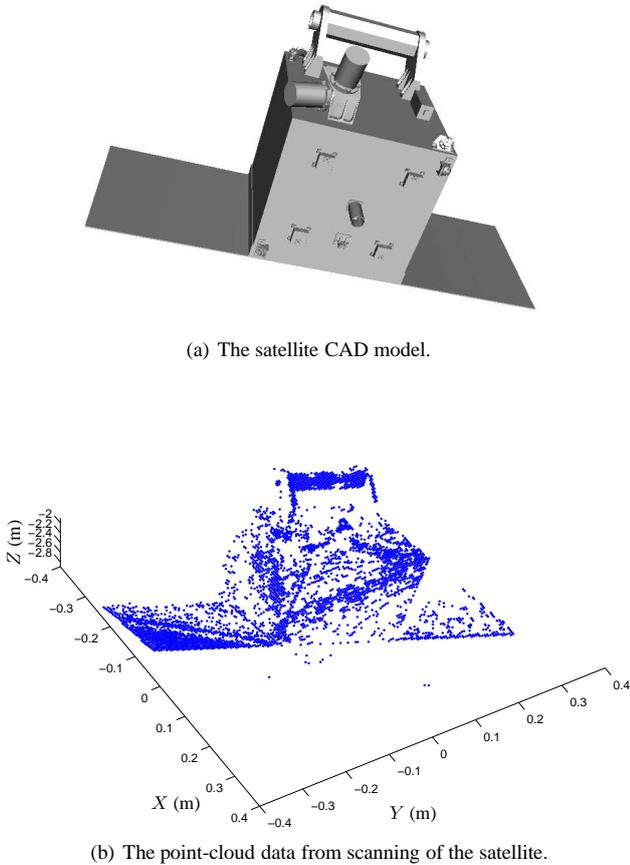(b) The point-cloud data from scanning of the satellite.

Figure 4: Matching points from the CAD model and the scanned data to estimate the satellite pose.

out KF in the loop.

Fig. 3 illustrates the experimental setup where a satellite mockup is attached to a manipulator arm, which is driven by a simulator according to orbital dynamics. The Neptec's Laser Camera System (LCS) [Samson et al., 2004], is used to obtain the pose measurements at a rate of 2 Hz. For the spacecraft simulator that drives the manipulator, parameters are selected as $I = \text{diag} \begin{bmatrix} 4 & 8 & 5 \end{bmatrix} \text{kgm}^2$ and $\rho_t^T = \begin{bmatrix} -0.15 & 0 & 0 \end{bmatrix}$ m. The solid model of the satellite mockup, Fig. 4(a), and the point-cloud data, generated by the laser camera system, Fig. 4(b), are used by the ICP algorithm to estimate the satellite pose according to the two schemes for providing the initial guess as shown in Fig. 2.

The robustness of the pose estimation of the moving satellite with and without incorporating the KF are illustrated in Figs 5 and 6, respectively. It is evident from Figs. 5(a) and 5(b) that the ICP-based pose estimation is fragile if the initial guess is taken from the last estimated pose. This will cause growing ICP fit metric over time, as shown in Fig. 5(c), that eventually lead to a total failure at $t = 90$ sec. On the other hand, the pose estimation with ICP and the KF in the closed loop configuration exhibits robustness as shown in Figs. 6(a) and 6(b). Trajectories of the estimated angular velocities obtained from the KF versus the actual trajectories calculated by using the manipulator kinematics are illustrated in Fig. 7. The plot shows that the estimator converges at around $t = 15$ sec.
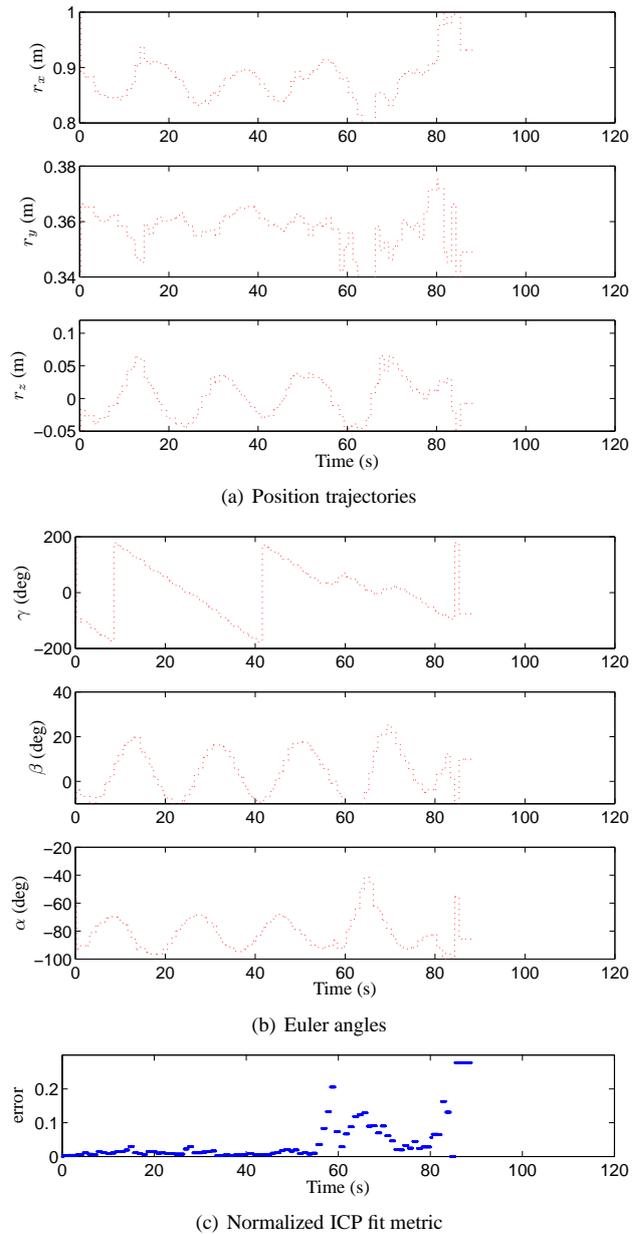

(a) Position trajectories
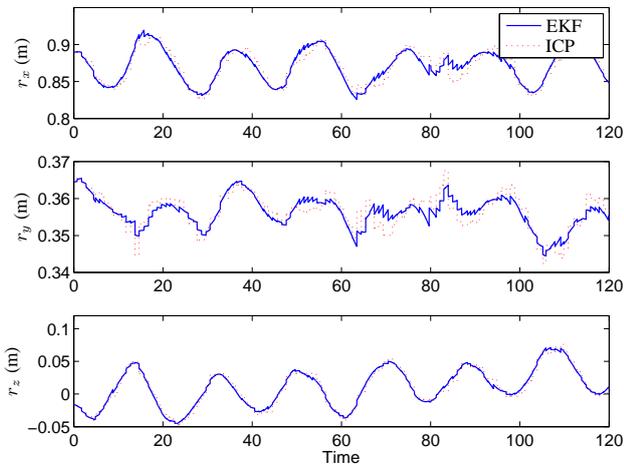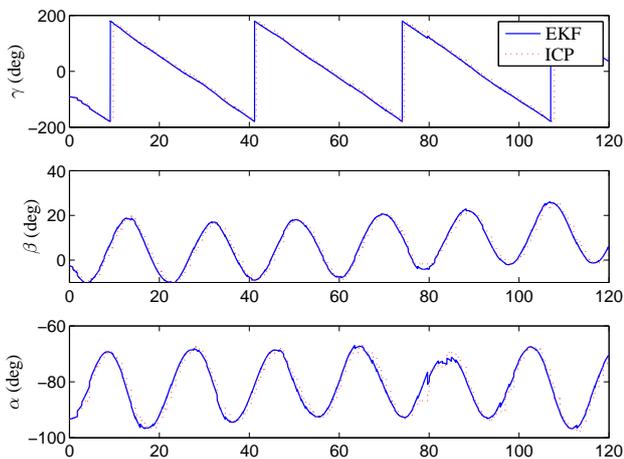

(b) Euler angles

(c) Normalized ICP fit metric

Figure 5: Pose estimation without incorporating EKF
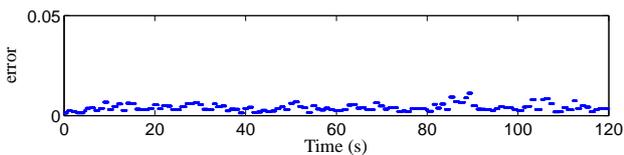
6 CONCLUSION

A method for pose estimation of free-floating space objects by incorporating a dynamic estimator in the ICP algorithm has been presented. An adaptive extended Kalman filter was used for estimating the relative pose of two free-falling satellites that move in close orbits near each other using position and orientation data provided by a laser vision system. Not only does the filter estimate the system states, but also all the dynamics parameters of the target. Experimental results obtained from scanning a moving satellite mockup demonstrated that the pose tracking based on ICP alone was fragile and did not converge. On the other hand, the integration scheme of the KF and ICP yielded a robust pose tracking.

(a) Position trajectories

(b) Euler angles

(c) Normalized ICP fit metric

Figure 6: Pose estimation with the closed loop ICP-EKF

REFERENCES

Aghili, F. and Parsa, K., 2009. Motion and parameter estimation of space objetcs using laser-vision data. AIAA Journal of Guidance, Control, and Dynamics 32(2), pp. 537–459.

Amor, B. B., Ardabilian, M. and Chen, L., 2006. New experiments on icp-based 3d face recognition and authentication. In: IEEE Int. Conference on Pattern Recofgnition, Hong Kong, pp. 1195–1199.

Besl, P. J. and McKay, N. D., 1992. A method for registration of 3-d shapes. IEEE Trans. on Pattern Analysis & Machine Intelligence 14(2), pp. 239–256.
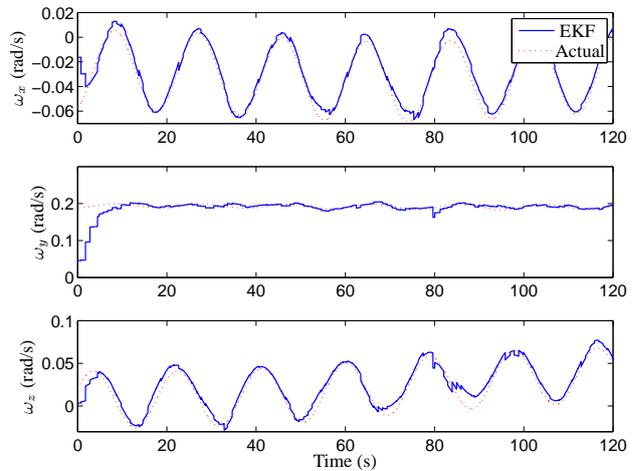
Figure 7: Angular velocities

Breakwell, J. and Roberson, R., 1970. Oribtal and attitude dynamics. Lecture notes.

Faugeras, O. D. and Herbert, M., 1986. The representation, recognition, and locating of 3-d objects. The International Journal of Robotics Research 5(3), pp. 27–52.

Kaplan, M. H., 1976. Modern Spacecraft Dynamics and Control. Wiley, New York.

Lefferts, E. J., Markley, F. L. and Shuster, M. D., 1982. Kalman filtering for spacecraft attitude estimation. Journal of Guidance 5(5), pp. 417–429.

Lichter, M. D. and Dubowsky, S., 2004. State, shape, and parameter esitmation of space object from range images. In: IEEE Int. Conf. On Robotics & Automation, New Orleans, pp. 2974–2979.

Masutani, Y., Iwatsu, T. and Miyazaki, F., 1994. Motion estimation of unknown rigid body under no external forces and moments. In: IEEE Int. Conf. on Robotics & Automation, San Diego, pp. 1066–1072.

Rekleitis, I., Martin, E., Rouleau, G., L'Archevêque, R., Parsa, K. and Dupuis, E., 2007. Autonomous capture of a tumbling satellite. Journal of Field Robotics, Special Issue on Space Robotics 24(4), pp. 275–296.

Samson, C., English, C., Deslauriers, A., Christie, I., Blais, F. and Ferrie, F., 2004. Neptec 3D laser camera system: From space mision STS-105 to terrestrial applications. Canadian Aeronautics and Space Journal 50(2), pp. 115–123.

Simon, D. A., Herbert, M. and Kanade, T., 1994. Real-time 3-d estimation using a high-speed range sensor. In: IEEE Int. Conference on Robotics & Automation, San Diego, CA, pp. 2235–2241.

Yoshida, K., 2003. Engineering test satellite VII flight experiment for space robot dynamics and control: Theories on laboratory test beds ten years ago, now in orbit. The Int. Journal of Robortics Research 22(5), pp. 321–335.

Zimpfer, D. and Spehar, P., 1996. STS-71 Shuttle/MIR GNC mission overview. In: Advances in Astronautical Sciences, American Astronautical Society, San Diego, CA, pp. 441–460.